УДК 551.322:548.2

Steady-state size distribution of air bubbles in polar ice

© 2014 г. V.Ya. Lipenkov[1], A.N. Salamatin[2]
[1]Arctic and Antarctic Research Institute, St.-Petersburg; [2]Kazan (Volga Region) Federal University
lipenkov@aari.ru

Установившееся распределение пузырьков воздуха по размерам в рекристаллизационном льду

В.Я. Липенков[1], А.Н. Саламатин[2]
[1]Арктический и Антарктический научно-исследовательский институт, Санкт-Петербург;
[2]Казанский (Приволжский) федеральный университет

Статья принята к печати 18 сентября 2014 г.

Air bubbles, geometrical properties, ice core, paleoclimate reconstruction, polar ice, size distribution.
Геометрические свойства, ледяной керн, палеоклиматическая реконструкция, пузырьки воздуха, распределение по размерам, рекристаллизационный лёд.

Between the close-off depth and the bubble-to-hydrate transition zone in polar ice sheets, the geometrical properties of air bubbles, such as number concentration and size of bubbles, are mainly controlled by firn temperature and ice accumulation rate prevailing during the snow to ice transformation [3], and by the bubble compression in the course of bubbly ice densification [13]. This implies that the data on the bubble properties can be used for reconstruction of the past climate change. On the basis of our earlier studies of bubbly ice densification and the new measurements of air bubbles in the Antarctic ice cores, we have developed a theory of bubble evolution in polar ice and propose an inverse procedure for bubble size conversion to specified conditions at the close-off depth. Both outcomes of the research contribute to elaboration of the new paleoclimatological tool based on the bubble properties.

List of symbols

b	accumulation rate
c	ice porosity (volume fraction of bubbles)
$F(r)$	probability density function of bubble-size (r) distribution
$f(r, p)$	probability density function of bubble-size (r) and pressure (p) distribution
h	depth
L	total length of pores per unit mass of ice
l	size of ice grains (grain edge length)
N	number of bubbles after their disintegration per unit mass of ice
p	gas pressure in a bubble
p_l	load pressure
r	radius of a bubble
r_p	radius of pores and elongated bubbles
s	coefficient of variation of bubble radii r
T	temperature
t	time
U	volume of a unit cell
V	total gas content of ice
v	volume of a bubble
y	number of pores per grain
α	length/radius ratio of cylindrical bubbles
φ_v	volume/edge length ratio of polyhedron chosen for ice grain approximation
ω	compression rate of a bubble
ρ_i	density of pure ice
ζ	r_d/r ratio
ζ'	r_c/r ratio
$\langle x \rangle$	mean value of variable x
$\sigma(x)$	standard deviation of variable x

Subscripts

c	close-off characteristic
d	characteristic at the end of bubble disintegration
trans	characteristic at the beginning of the bubble-to-hydrate transition zone
0	standard conditions (STP).

Introduction

Polar ice cores have for a long time been recognized as an invaluable source of data on past climate and atmosphere history. Traditionally most of the paleoclimatic information comes from the analyses of water isotopes, entrapped atmospheric air, and soluble and insoluble impurities in ice. However, some of the physical properties of ice itself can also be used as a supplementary and independent source of paleoclimatic data. In particular, the geometrical properties of air inclusions in ice are thought to store information about past temperature and accumulation rate. Earlier studies [1] revealed climate-related variations in air-bubble sizes and number concentrations at different depths in the Vostok ice core. The updated experimental profiles of air bubble properties at Vostok ([1, 12] and newly obtained data) are shown in Fig. 1 along with the ice isotope record [10]. The data demonstrate that the sizes (number concentrations) of bubbles are smaller (greater) in ice formed under the full glacial conditions (the Last Glacial Maximum or LGM) than in Holocene ice.

The link between bubbles and climate can be understood if one takes into account that bubble sizes and number concentrations are primarily controlled by grain sizes at the pore close-off depth, as was first proposed by A. Gow [8] and quantitatively demonstrated in subsequent publications [3, 12, 28]. The grain size at this depth is in turn a function of the grain-growth rate (depends mainly on the firn temperature), and the age of ice at pore close-off controlled by densification process (which is temperature and accumulation dependent [21]). Accordingly, the geometrical properties of bubbles at any depths between the pore close-off and the bubble-to-hydrate transition (500–1250 m at present time at Vostok [12]) are mainly controlled by firn temperature and ice accumulation rate prevailing during the snow to ice transformation [3], and by the bubble compression in the course of bubbly ice densification [13, 19]. Hence, before using the bubble size record for paleoclimate reconstruction, one has to reduce the bubble sizes measured at different depths to the close-off conditions. With this in mind, we develop here a model which describes the evolution of the bubble-size distribution with depth and allows us to reduce the sizes of compressed air bubbles to the original conditions prevailing at the close-off depth during bubble formation.

Formation of bubble ensembles in polar ice

In dry snow, a structural re-arrangement of ice grains by linear-viscous boundary sliding is a dominant mechanism of densification [5]. When snow reaches a relative density of about 0.6–0.7, the coordination number of grains (number of contacts per grain) approaches 6–7, thus, making the sliding impossible. Deformation of grains by power-law creep allows further densification of firn leading to further increase in the number of contacts per grain and growth of the average contact area [7, 22, 23]. As a result, when firn reaches a relative density of 0.8, the pores are reduced to thin cylinders going along the ice-grain edges, whereas the grains are similar by shape to equilibrium space-filling polyhedrons of the type of Kelvin's or Williams' tetrakaidecahedron [14].

Owing to curvature and surface tension the cylindrical pores in ice are unstable with respect to their disintegration into a number of spherical bubbles (see e.g., [25]). The plastic deformation of grains, the ice-grain growth, and the disintegration (pinch-off) of pores are the three processes that acting simultaneously control the dynamics of pore closure and air trapping in firn [6].

Because of percolation and sometimes sealing effects, the air becomes isolated from the atmosphere few meters above the depth at which zero open porosity is observed from the porosity measurements done on small samples of firn [15, 29]. However, regarding macro-scale in-situ properties of polar firn, both the air isolation in terms of pressure and the actual pore closure occur simultaneously at the same depth level hereafter referred to as «close-off depth» and denoted by h_c. The amount of air trapped at this level determines the air content of ice. Thus, the firn porosity at which the air is isolated and the close-off depth can be estimated from the air content of recent ice and the experimental porosity/density profile, provided the atmospheric pressure and the firn temperature are known [15].

Further development of bubble ensemble below h_c involves post-closure disintegration of isolated pores and elongated bubbles and compression of all air inclusions in plastically deforming ice matrix driven by the pressure lag between the two phases. By definition, the disintegration alone does not affect the volume concentration of air in ice, but tends to increase the number of bubbles. The process persists until the length/radius ratio, α, of all cylindrical bubbles is reduced to about 2π [25]. In the case of Vostok this condition is satisfied at about 160–170-m depth (60–70 m below pore close-off). However, «isometric» bubbles (i.e. bubbles with $\alpha \leqslant 2\pi$) represent up to 50% of the total bubble population already at 105 m and up to 80% at 110 m, whereas α of remaining elongated inclusions at 110-m depth rarely exceeds 4π. Thus, the number of bubbles in sinking ice is mainly determined within a narrow depth interval of the first tens of meters below h_c, where radius r_p of elongated inclusions still remains within a few percent of pore radius r_{pc} at the close-off depth.

Based on the above consideration, we postulate that at the end of bubble disintegration the number of isometric bubbles per unit mass of ice, N, is proportional to the length/radius ratio of firn pores at the close-off depth:

$$N = L_c/\alpha r_{pc}, \tag{1}$$

where L_c is the total length of pores per unit mass of ice at the close-off depth. With this assumption, it was deduced [3] that the number of bubbles in polar ice is linked to the grain size at the close-off depth as

$$N = G/l_c^3, \qquad G = \frac{\sqrt{\pi}}{\alpha\rho_i}\left(\frac{y}{\varphi_v}\right)^{1.5}\left(\frac{1-c_c}{c_c}\right)^{0.5}. \tag{2}$$

Here y is the number of pores per grain, and the value of φ_v is specified by the type of regular polyhedrons chosen for ice-grain approximation, ρ_i is the density of pure ice; α is assumed to be a constant parameter which refers to a preferred wavelength of bubble surface per-

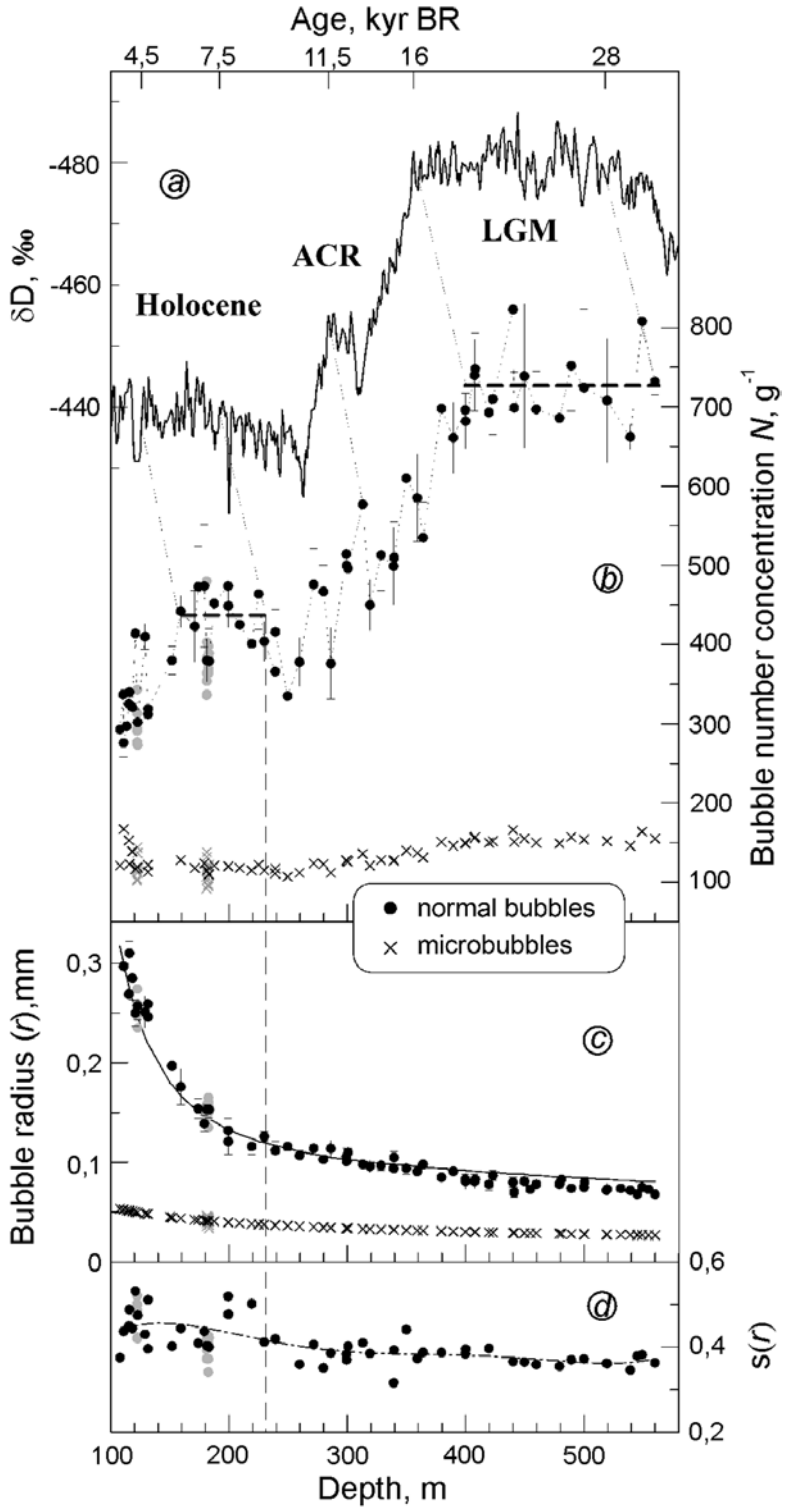

Fig. 1. Variations of the geometrical properties of air bubbles with depth in the Vostok ice core:
a – the deuterium record from the Vostok ice core indicating the local surface temperature change [10]. The δD axis is inverted to facilitate comparison with the experimental profile of the number concentration of air bubbles in ice; *b* – number of normal bubbles and microbubbles in 1 g of ice, *N*. Vertical bars indicate variability of the normal bubble concentrations within 9 cm thick ice core layer; *c* – mean radii ⟨*r*⟩ of normal bubbles (measured) and microbubbles (calculated using the data on microbubbles at 183 m depth). Vertical bars for ⟨*r*⟩ of normal bubbles as in *b*. The solid curve was calculated from the data on normal bubbles at 183 m depth assuming steady-state conditions; *d* – coefficient of bubble radii variation, *s*(*r*). Grey symbols in *b, c, d* show results of continues measurements within 1 m long ice core increments. Because of the difference in the ages of ice and entrapped bubbles, the climate-related variations in the bubble records are observed somewhat deeper than the corresponding variations in

turbation and thus determines the average size and the number concentration of future spherical bubbles for a given porosity c_c and grain size l_c at pore closure.

From theoretical [27] and experimental [30] studies it follows that the bubble migration under temperature gradients typical for polar ice sheets cannot significantly affect the initial bubble concentrations. In the absence of rapid ice deformation, the effects of both bubble coalescence due to bubble collisions [31] and bubble splitting «owing to the differing deformation in neighboring grains» [4] are negligibly small. The probability of bubble coalescence associated with ice-grain growth is also considered to be low because of the small size of bubbles and a tendency to bubble-boundary separation which, as a rule, occurs below the close-off depth [8].

Finally, the data from polar ice cores [1, 9, 17] show that the mean bubble concentration doesn't change with depth h at stationary (Holocene) conditions (see also Fig. 1). It is therefore reasonable to assume that, from the end of bubble disintegration ($h = h_d$) to the upper boundary of the bubble-hydrate transition zone ($h = h_{trans}$), the number of bubbles in a reference ice particle remains fixed. In this section of ice sheet, bubble compression is the only process that governs the evolution of bubble-size distribution with depth and controls the geometrical properties of bubble ensembles in sinking ice.

Evolution model of the bubble-size distribution (from the end of bubble disintegration to the beginning of bubble-hydrate transition)

Observations show that neither the radii of real pores nor the grain sizes are uniform at pore close-off. In addition, under the same load pressure, the rate of grain deformation depends on the grain contact area which determines the effective stress acting on contact flats (e.g., [14]). Therefore, the compression of closed pores and bubbles in firn is expected to be an inhomogeneous process on the micro-scale level. Because of these and other complexities a bubble ensemble forming below close-off is not uniform with respect to size and gas pressure of the inclusions [8, 12, 13].

In what follows, we confine our consideration to the depth range $h_d < h < h_{trans}$. The number of bubbles N in a sinking ice particle is fixed, and the bubble ensemble at a certain depth level (or instant in time) is characterized by the probability density function of bubble size and pressure distribution $f(r, p)$ which, by definition, determines the number of bubbles dN whose equivalent-sphere radii and pressures fall into the intervals from r to $r + dr$ and from p to $p + dp$, respectively:

$$dN = N f(r, p) dr dp.$$

Available data on air bubbles in polar ice cores are mostly restricted to the experimental bubble-size distributions. The corresponding probability density function, $F(r)$, is

$$F(r) = \int f(r, p) dp.$$

The time evolution of the bubble-size distribution in a reference ice particle, described by $F(t, r)$, results from compression of bubbles in ice matrix plastically deforming under load pressure p_l . The driving force here is the pressure lag $p_l - p$ unique for each bubble. To develop a model for bubble ensemble evolution, we introduce the compression rate of a bubble as

$$\omega = -\frac{1}{v}\frac{dv}{dt} = -\frac{3}{r}\frac{dr}{dt}, \qquad (3)$$

where v is the volume of a spherical bubble, and d/dt designates hereafter the particle derivative of a variable.

Because the ice porosity is small (< 0.1) and the bubbles are scarce at these depths, we can divide ice matrix into a number of cells U, each containing a single bubble

the deuterium record. The thin dashed lines connect the synchronous events in the records. LGM – Last Glacial Maximum; ACR – Antarctic Cold Reversal. The ice age at the top axis is from [20]

Рис. 1. Изменение по глубине геометрических характеристик включений воздуха в керне со станции Восток:
a – профиль изотопного состава керна по дейтерию, характеризующий изменение температуры на поверхности ледника [10]. Ось δD перевёрнута для облегчения сравнения с профилем счётной концентрации включений во льду; *b* – количество гипогенных включений воздуха и автогенных микропузырьков в 1 г ледяной породы, *N*. Вертикальными отрезками показаны пределы изменчивости *N* гипогенных включений в пределах 9-сантиметровых слоёв ледяного керна; *c* – средние радиусы ⟨*r*⟩ гипогенных включений (результаты измерений) и автогенных микропузырьков (расчёт на основании данных, полученных на горизонте 183 м). Пределы изменчивости размеров гипогенных пузырьков (как на рис. *b*) показаны вертикальными отрезками. Сплошная линия – размер гипогенных включений, рассчитанный по данным их измерений на горизонте 183 м, исходя из предположения о стационарности условий льдообразования; *d* – коэффициент вариации радиусов гипогенных включений, *s*(*r*). Значения, показанные на рис. *b*, *c*, *d* серым цветом – результаты непрерывных послойных измерений характеристик включений в пределах интервалов керна длиной 1 м. Поскольку возраст гипогенных включений (отсчитывается с момента их изоляции от атмосферы) меньше возраста вмещающего их льда (отсчитывается с момента отложения снега на поверхности ледника), климатически обусловленные вариации в профилях характеристик включений воздуха наблюдаются несколько глубже соответствующих вариаций в профиле δD. Синхронные вариации на профилях соединены пунктирными линиями. Возраст льда на верхней шкале дан по данным работы [20]

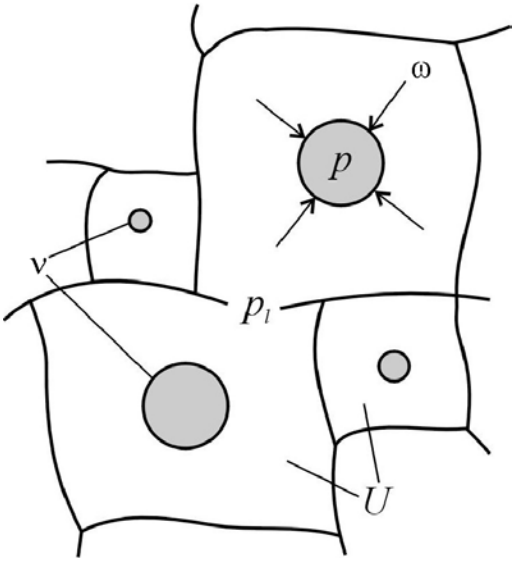

Fig. 2. Schematic of the compression of single bubbles in the polydisperse bubble-ice system (see text for explanations)
Рис. 2. Схема, иллюстрирующая процесс сжатия отдельных включений в полидисперсной системе лёд – пузырьки воздуха (см. текст)

and deforming as a volume of constant mass (see Fig. 2). Consequently, for incompressible ice we have

$$\frac{dv}{dt} = \frac{dU}{dt}. \tag{4}$$

For each bubble the cell is chosen so as to provide the cinematic consistency of the cell ensemble deformation. This implies that the compression rates of different cells are identical and equal to the averaged (macro-scale) compression rate of bubbly ice:

$$\frac{1}{U}\frac{dU}{dt} = -c\bar{\omega}, \tag{5}$$

where by definition $\bar{\omega} = <\omega v>/<v>$, and c is the volume concentration of bubbles (ice porosity).

Combining Equations (3)–(5), the volume U of each cell is determined by

$$v/U = c\bar{\omega}/\omega,$$

which means that (at least for small c) the compression of a single bubble of volume v and pressure p in the *polydisperse* bubble-ice system is identical with that in the *periodic* (*monodisperse*) bubble-ice cell structure with the apparent bubble-volume concentration equal to $c\bar{\omega}/\omega$.

Rheological behavior of *periodic* bubbly media was theoretically studied by Salamatin and Duval [18], and then used by Salamatin with coauthors [19] to construct a densification model for bubbly ice represented as a periodic structure. Substituting $c\bar{\omega}/\omega$ into the latter theory instead of c, one obtains (see Appendix) an integral relation linking the compression rate of a single inclusion in the *polydisperse* bubble-ice system to the corresponding pressure drop:

$$p_l - p = \varphi(\omega; c, \bar{\omega}, ...). \tag{6}$$

Assuming mass exchange between the two phases is negligible, the ideal-gas state equation for each bubble yields

$$pv/T = p_0 v_0/T_0. \tag{7}$$

Here T (K) is the current temperature of the ice particle, and v_0 is the volume of dry air in the bubble at standard conditions (STP). The latter quantity (constant for each bubble) is determined by the thermodynamic conditions at pore close-off, so that on average $\langle v_0 \rangle = V/N$, where V is the total gas content of ice.

Equations (3), (6), (7) form a simultaneous system for simulating temporal changes in pressures and volumes of individual air bubbles. They are similar to the equations which describe the bubbly-ice densification in terms of the averaged characteristics: c, $\bar{\omega}$, $\bar{p}$, where $\bar{p} = \langle pv \rangle/\langle v \rangle$ is the volume-weighted bubble pressure (see Appendix). Computational experiments [19] showed that the pressure evolution and the rate of compression in the bubble ensemble insignificantly depend on the initial conditions at pore close-off. In the upper part of the bubbly-ice stratum, pressures p (although different from one bubble to another) are uniformly small with respect to the load pressure p_l and, in accordance with Equation (6), variations in the compression rate ω of different bubbles are small too. Deeper in the ice sheet, in the asymptotic phase of bubbly-ice densification, the pressure in all bubbles equalizes. The latter has been confirmed by direct measurements of the bubble pressure in the Vostok ice core [13]. Consequently, in spite of a considerable difference in bubble sizes, their compression rates $\omega \approx \bar{\omega}$, and therefore the evolution of the bubble volumes (radii) in the depth range of interest can be calculated with sufficient accuracy by using Equations (3), (6), at (7) at $p = \bar{p}$.

Based on this approximation and designating by the subscript «d» characteristics of a bubbly-ice particle at the end of the disintegration zone (h_d), for any time $t > t_d$, when the particle reaches a depth h, from Equation (7) we write

$$\frac{r_d}{r} = \left(\frac{\bar{p} T_d}{T \bar{p}_d} \right)^{\frac{1}{3}} = \zeta. \tag{8}$$

Here $\zeta = \zeta(t)$ is a function of time. The number of bubbles in the ice particle remains constant and for any sub-ensemble (dN) it holds

$$F(r)dr = F_d(r_d)dr_d. \quad (9)$$

Combining Equations (8) and (9), yields

$$F(t,r) = \zeta(t)F_d(r\zeta(t)). \quad (10)$$

Hence, after completion of bubble disintegration, the form of the bubble-size distribution in a sinking ice particle is expected to remain time-invariant, and, as a consequence, the coefficient of variation, s, equals that at the end of disintegration ($s = s_d$). In this case a simple scaling procedure based on Equations (8) and (10) would be sufficient to make the distributions obtained at different depths coinciding with each other, provided the ice formation conditions (the initial properties of bubble ensembles at $h = h_d$) were steady-state and did not change. The mean bubble pressure, $\bar{p}$, should be simulated using the ice densification model [19], as explained in Appendix.

The s-depth profile shown in Fig. 1, d does support a constancy of the relative variance of bubble radii within the ice strata formed under stationary (either Holocene or LGM) conditions. More detailed discussion of the bubble-size distribution is presented in the next section where we examine the above theoretical results using an extensive set of data obtained from Vostok and other polar ice cores.

Experimental data

The ice cores used in this study were retrieved from the deep boreholes 3G, 4G, and 5G drilled at Vostok Station as well as from a number of shallower holes drilled along the traverse route Mirny – Vostok and named by the distance in kilometers from Mirny Observatory: KM 140, KM 260, KM 325, KM 400, and at Komsomolskaya Station (KMS). The measurements were performed on unrelaxed ice, that is either on the fresh ice core soon after drilling, or on ice samples stored at a temperature of −55±2 °C, which is low enough to prevent (at least during the first 5 years after ice recovery) significant decompression of air bubbles [2].

Thick sections for bubble studies were cut along the core axis that represented continuous 9-cm increments of the core length (or 4 to 40 years' accumulation, depending on site and depth). The upper and lower surfaces of each thick section were microtomed and then polished with a small amount of alcohol. Silicone oil was applied to avoid air between the ice slice and the glass plate to which it was attached with supercooled water drops, as well as to prevent sublimation from the upper surface of the slice. The thickness of the thick sections was kept at about 2–4 mm during the inclusion-size measurements, and then thinned down to 1–2 mm before counting the number of inclusions. The thick sections were analyzed under a binocular microscope in the field laboratory at −12 °C as described in [12].

Besides the original measurements, available published data from the Dye 3 ice core drilled in Greenland [26], and the Byrd core from Antarctica [8, 9] were also used in our analysis.

The geometrical properties of the bubble populations in the studied ice samples (or ice particle) from different depths are described by the number concentration N and the size distributions of air inclusions. The size of each bubble is expressed by equivalent-sphere radius r while the whole population is characterized by the mean value, $\langle r \rangle$, the standard deviation $\sigma(r)$ of bubble radii, and the coefficient of variation, s, defined as $s = \sigma(r)/\langle r \rangle$. It should be noted that s is also the standard deviation of relative bubble radii $s \equiv \sigma(r/\langle r \rangle)$, and in the case of the log-normal size distribution, its value is typically within a few percent of the logarithmic standard deviation $\sigma(\ln r)$, or precisely: $\sigma^2(\ln r) = \ln(1 + s^2)$.

At least 200 inclusions were measured in each thin section to obtain statistically representative data on their size distribution. Both normal bubbles formed due to pore closure and microbubbles entrapped by growing ice grains in the shallower section of firn [12] were analyzed. The results obtained on the Vostok ice cores are shown in Fig. 1. In the following consideration we only use data for normal bubbles.

Applying theory to the data

Equations (8) and (10) can be easily transformed to calculate the initial bubble-size distribution function $F_d(r_d)$ from the experimental distribution $F(r)$ obtained at any depth h between h_d and h_{trans}. However, by the end of disintegration, air bubbles have already experienced significant compression and therefore their sizes, according to Equation (7), additionally depend on the temperature T_c and atmospheric pressure p_c at pore isolation. A more appropriate reference level for comparing bubble ensembles formed under different climatic conditions is then the close-off depth, h_c, at which the ice-grain texture solely determines the geometrical properties of trapped bubbles.

Extension of the bubble-evolution model up to the close-off depth. For characterizing the bubble sizes at h_c, it is convenient to mentally replace a complicated system of elongated, often ramified, gas inclusions

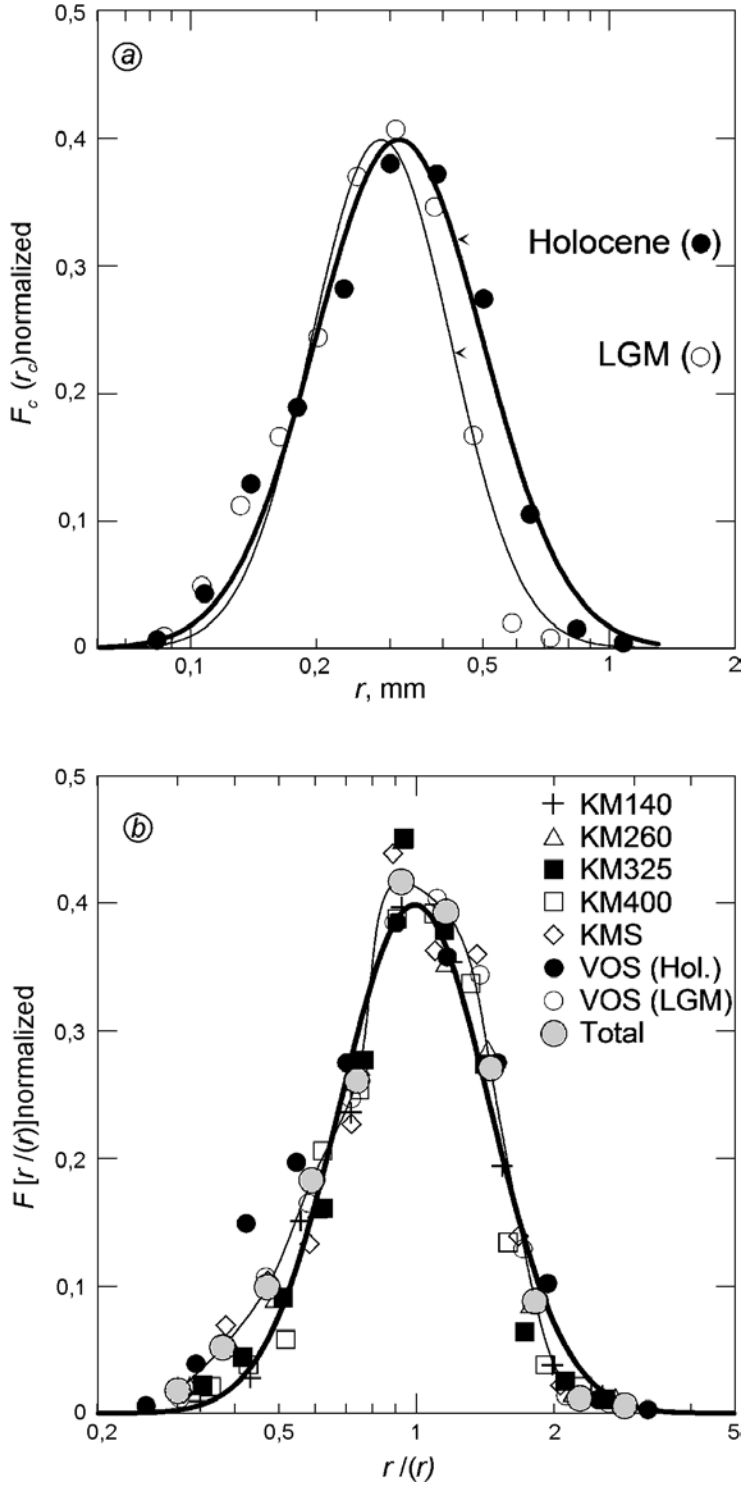

Fig. 3. The stacked bubble-size distributions in the Holocene and LGM ice strata:
a – the stacked size distributions for Holocene and LGM bubble populations in the Vostok ice core. The Holocene (LGM) stack is based on 2000 (2400) bubbles measured at 10 (13) depth levels in the depth range 160–225 m (400–560 m). The experimental distributions from different depths were reduced to the corresponding close-off conditions as described in text. The best-fit log-normal functions are also shown for comparison; *b* – the stacked distributions of relative bubble radii in Holocene ice at six drilling sites in Antarctica and in LGM ice at Vostok are shown by symbols as indicated in the figure. The thin curve represents the total-stack distribution based on 11000 bubbles. The thick curve is a log-normal distribution fitted to the total stack. (In each case a normalized probability density is defined as $F(x)_{norm} = dN/(NdX)$, $X = (\ln x - \langle \ln x \rangle)/\sigma(\ln x)$, where x stands for either r or $r/\langle r \rangle$; a log-normal function is given

typical at this depth by an equivalent system of isometric (spherical) bubbles that would exist here if the disintegration occurred at the same time as the pores closed. Such a fictitious bubble ensemble is characterized by the same volume concentration of inclusions as the real one. However, the number concentration and the distribution of the relative radii of the bubbles are the same as those which will be acquired by the bubble ensemble after the bubbles have disintegrated. The size distribution of spherical bubbles at pore close-off, $F_c(r_c)$, can be deduced from the bubble sizes measured below the disintegration zone using analogues of Equations (8) and (10)

$$F_c(r_c) = F(r_c/\zeta')/\zeta', \qquad r_c / r = \left(\frac{\bar{p} T_c}{T p_c} \right)^{\frac{1}{3}} = \zeta'. \qquad (11)$$

The mean value and the coefficient of variation of bubble radii are $\langle r_c \rangle = \zeta' \langle r \rangle$, and $s_c = s$, respectively.

The average bubble pressure $\bar{p}$ in Equation (11) is predicted by the ice densification model [19]. In contrast to our previous work [13], we now employ this model with the boundary conditions (T_c, p_c, c_c, ...) which refer to the new, air-content-based definition of the close-off depth described above. As might be expected, after rising the upper boundary of bubbly ice typically by 2 to 6 m, we do not observe any appreciable change in the best-fit values of the main model parameters (rheological properties and air content of ice) as compared to those established for the same drilling sites under the old, closed-porosity-based definition of the close-off depth [13].

Our own experience with ice samples from Vostok and Komsomolskaya show that predominance of elongated inclusions, even at the coldest sites, is restricted to the first ten meters of bubbly ice. We therefore do not attempt to incorporate in the model a «cylindrical approximation» of air bubbles [32] in order to improve simulation of bubble pressures in the narrow depth range where the evolution of inclusion shape essentially takes place. Judging from the computational experiments [13], the actual instability of the close-off conditions (in particular those which determine the air content of ice) appears to be more crucial for fitting the model to the data than other uncertainties of the modeling.

Steady-state bubble-size distribution. Using the second of Equations (11) we reduced the sizes of normal bubbles measured at different depths within Holocene (160–225 m) and LGM (400–560 m) sections of the Vostok core to the corresponding close-off conditions. For Holocene at Vostok we took the present-day values of T_c and p_c, whereas for LGM we estimated: $T_c = 205 \pm 1$ K (-68 ± 1 °C), $p_c = 0.065 \pm 0.002$ MPa from the available paleoclimatic reconstructions [11, 16, 19]. Because the log-normal bubble-size distribution was expected [1], the calculated bubble radii r_c were recollected in logarithmic bins. Then a conventional normalization of the probability density function $F_c(r_c)$ with respect to the logarithmic standard deviation $\sigma(\ln r_c)$ was applied in order to have a constant height of the distribution plots. The resulting stacked size distributions for Holocene and LGM bubble populations in Vostok ice are shown in Fig. 3, *a* together with their log-normal fits. Despite considerable differences in the bubble number concentrations (435 g^{-1} in Holocene ice versus 735 g^{-1} in LGM ice), and the mean bubble radii at pore close-off (0.33 mm and 0.28 mm, respectively), both of the experimental stacks closely correspond with a log-normal distribution function. The width of the distribution, however, changes from $s = 0.43$ in Holocene ice to $s = 0.37$ in LGM ice. The data on $\langle r_c \rangle$, s, and N for Vostok and other cores are given in Table.

Equations (8) and (10) imply a fixed distribution of relative bubble sizes after completion of bubble disinte-

by $F(x)_{norm} = (2\pi)^{-0.5}\exp(-X^2/2)$.) KMS stands for Komsomolskaya, VOS – for Vostok Station; «Total» is the total-stack distribution based on 11000 bubbles from all studied sites

Рис. 3. Сводные распределения включений воздуха по размерам в слоях льда, сформировавшихся в голоцене и в период последнего максимума оледенения (ПМО).

a – сводные распределения включений воздуха для голоцена и ПМО по результатам исследований керна со станции Восток. Распределение для голоцена (ПМО) основано на измерениях 2000 (2400) включений на 10 (13) горизонтах ледниковой толщи в интервале глубин 160–225 м (400–560 м). Экспериментальные распределения, полученные на разных глубинах, приведены к условиям на уровне замыкания пор, характерным для голоцена и ПМО, по методике, описанной в тексте. На рисунке также показана кривая логнормального распределения, наилучшим образом аппроксимирующая экспериментальные данные; *b* – сводные распределения нормированных радиусов воздушных включений в голоценовом льду в шести пунктах бурения в Антарктиде и во льду ПМО в районе станции Восток. Тонкая кривая – общее сводное распределение, основанное на измерениях 11 тыс. пузырьков воздуха; жирная кривая – логнормальное распределение, соответствующее экспериментальным данным. В каждом случае нормированная плотность вероятности определялась как $F(x)_{norm} = dN/(NdX)$, $X = (\ln x - \langle \ln x \rangle)/\sigma(\ln x)$, где x обозначает r или $r/\langle r \rangle$; логнормальная функция определяется как $F(x)_{norm} = (2\pi)^{-0,5}\exp(-X^2/2)$.) KMS, VOS – данные по кернам станций Комсомольская и Восток соответственно. «Total» – общее сводное экспериментальное распределение, построенное по измерениям 11 тыс. пузырьков во всех изученных кернах

Characteristics of air bubbles in polar ice as related to the ice formation conditions (temperature, T, and accumulation rate, b)
Геометрические параметры газовых пузырьков в различных условиях рекристаллизационного льдообразования (температура T, скорость аккумуляции льда b)

Drilling site	Location	T, °C	b, g·cm^{-2}·yr^{-1}	N, g^{-1}	N error, g^{-1}	$\langle r_c \rangle$, mm	$\langle r_c \rangle$ error, mm	$s(r)$
Dye 3	65°11'N, 43°49'W	−20	50	300	±60	0.42	±0.05	
KM140	67°45'S, 93°39'E	−27	40.4*	345	±40	0.40	±0.04	0.35
Byrd	80°00'S, 120°00'W	−28.7	16	250	±40	0.43	±0.02	
KM260	68°46'S, 94°28'E	−33.5	6.9	270	±50	0.41	±0.02	0.37
KM325	69°18'S, 95°01'E	−37	14	380	±45	0.38	±0.02	0.35
KM400	69°57'S, 95°37'E	−39.9	15.4	485	±50	0.36	±0.02	0.33
Komsomolskaya	74°06'S, 97°30'E	−53.8	6.4	650	±15	0.30	±0.01	0.38
Vostok (Hol.)[9)]	78°28'S, 106°48'E	−57	2.1	435	±20	0.33	±0.01	0.43
Vostok (LGM)				725	±20	0.28	±0.01	0.37

gration. Thus, mixing together the relative radii $r/\langle r \rangle$ of air bubbles measured at different depths one can construct a representative stacked size distribution corresponding to given (steady-state) ice formation conditions. In Fig. 3, *b* we show such stacked distributions obtained for Holocene ice at six drilling sites located along the route Mirny – Vostok together with the LGM bubble-size distribution in the Vostok ice.

In general, the individual stacks for particular ice cores reveal close clustering around the total-stack distribution (thin curve in Fig 3, *b*) based on 11 000 bubbles from different sites and depths. Although fitting of some other distribution functions to the bubble data might be tested [1], an apparently good agreement between the «empirical law» (total stack) and the fitted log-normal distribution (bold curve in Fig. 3, *b*) indicate a sufficiency of log-normal function to describe the properties of air bubbles formed under different climatic conditions.

Given the steady-state bubble-size distribution in polar ice is log-normal, the values of $\langle r_c \rangle$, s and N, gathered in Table for a number of Holocene ice cores from Antarctica and Greenland, provide a total characteristic of the geometrical properties of the bubble populations as determined by the size of the ice grains at pore close-off in different climatic conditions. From $\langle r_c \rangle$, the mean bubble radius $\langle r \rangle$ can be calculated for any desired depth between h_d and h_{trans} as described above. The volume concentration c of log-normally-distributed inclusions can be calculated from relations [12, 24]:

$$c/(1-c) = (4/3)\pi\langle r\rangle^3 k^3 N\rho_i, \quad k = e^{\sigma^2(\ln r)} = 1 + s^2. \quad (12)$$

The uncertainties of $\langle r_c \rangle$ and N indicated in Table have been determined as 2σ-errors of the mean values obtained by averaging the results from the different depth levels. The error bars for the data adopted from literature (Dye 3 and Byrd ice cores) have been increased so as to cover additional uncertainties due to unreported details of the experimental procedures.

For different sites, the experimental values of s vary from 0.33 to 0.43 (see Table). The data, however, reveal no correlation between the width of the bubble-size distribution and the ice formation conditions. It is therefore reasonable to assume at this stage that the air bubbles formed in polar ice at different climates have similar (log-normal-like) distribution of relative radii with $s = 0.38\pm0.05$ or $\sigma(\ln r) = 0.37\pm0.05$, as shown in Fig. 3, *b*. The uncertainty resulting from using the above mean values in Equation (12) for estimating the mean radius (number concentration) of air bubbles from other known parameters of their population does not exceed 3% (10%).

Relationship between the size and number of air bubbles in polar ice. Fig. 4 shows variations of the bubble sizes at the close-off depth with number concentration of bubbles in ice below the disintegration zone (the data are from Table). The two dashed lines in the figure are calculated using Equation (12) with $s = 0.38$ ($k = 1.14$) and c_c set at 0.09 or 0.11 as indicated in the figure. The latter values bound the full present-day range of the close-off porosity in polar ice. There can be seen a tendency of the warmer (colder) sites to be located closer to the line corresponding to the higher (lower) porosity. However, this does not disguise much a clear linear correlation between reciprocal of cube of the mean bubble radius, $1/\langle r_c \rangle^3$, and the bubble number N which is expected from Equation (12) in the case when variability of c_c and s is comparatively small. In summary, the experimental data obtained from the Antarctic and Greenland ice cores seem to support the theory which we have developed to describe formation and evolution of bubble ensembles in polar ice.

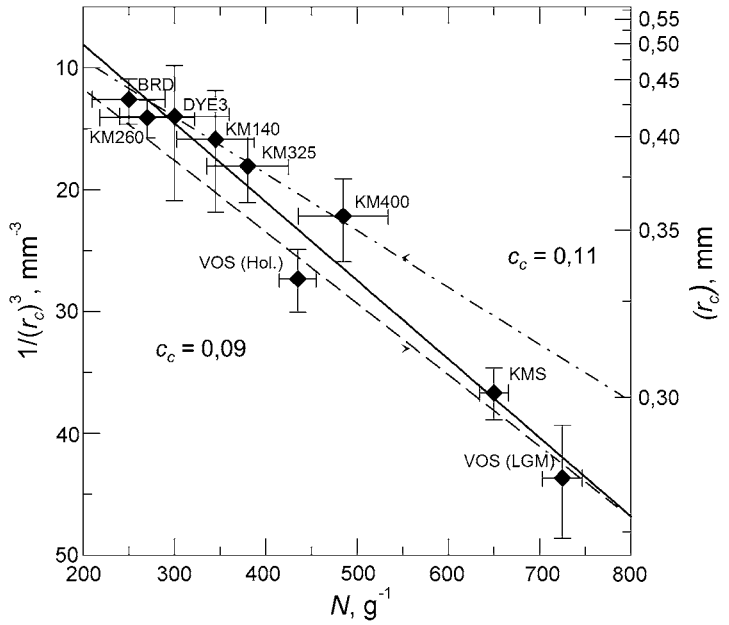

Fig. 4. The relation between the mean equivalent-sphere radius of air bubbles reduced to the close–off conditions, $\langle r_c \rangle$, and the number concentration of bubbles after disintegration, N.

The data and the error bars are from Table. The least-squares regression is shown by solid line. The two dashed lines are calculated using Equation (12) with $s = 0.38$ and c_c set at 0.09 and 0.11 as indicated in the Figure

Рис. 4. Связь эквивалентного радиуса гипогенных включений, приведённого к уровню границы фирн–лед $\langle r_c \rangle$ со счетной концентрацией включений после завершения их дезинтеграции N.

Экспериментальные данные из таблицы. Сплошной линией показана линейная регрессия, полученная методом наименьших квадратов; пунктирами – теоретические зависимости размера пузырьков от их количества во льду, рассчитанные по уравнению (12) для двух предельных значений пористости рекристаллизационного льда на границе фирн–лёд ($c_c = 0{,}09$ и $c_c = 0{,}11$) при $s = 0{,}38$

Conclusion

We have demonstrated that the shape of the bubble-size distribution after the completion of bubble disintegration does not depend on the climatic conditions of ice formation and remains self-similar in an ice particle sinking in polar ice sheet. Our theoretical inferences are supported by direct measurements of the bubble sizes at different depths within the Holocene ice formed under different ice-formation conditions at the eight drilling sites in Antarctica and Greenland, as well as in the LGM ice at Vostok.

The stacked distribution of bubble radii (the «empirical law») based on 11 000 measurements reveals sufficiently close agreement with log-normal distribution. This facilitates description of the geometrical properties of the bubble ensembles and provides a simple connection between the two climate-related properties of the inclusion – the number concentration and the mean size of bubbles. Moreover, it is shown that the air bubbles formed in polar ice at different climates are characterized by essentially the same steady-state (log-normal-like) distribution of relative radii with a standard deviation of 0.38±0.05.

On the basis of the obtained results we proposed a simple method for reduction of bubbles to the close-off conditions for recovery of the climatic signal imprinted in the bubble-size records obtained at the low-accumulation sites of polar ice sheets. The new developments contribute to the theory of formation and evolution of air bubbles in polar ice sheets above the bubble-to-hydrate transition zone and open the door to combined use of the two experimentally independent properties of bubbles as indicators of the past ice formation conditions, such as firn temperature and accumulation rate.

Acknowledgment. We thank D. Raynaud and P. Duval for valuable comments which have been taken into account in the final version of the paper.

The work was supported by the Russian Foundation for Basic Researches, Grant 06-05-65174.

References

1. *Барков Н.И., Липенков В.Я.* Количественная характеристика структуры льда в районе станции Восток до глубины 1400 м // МГИ. 1984. Вып. 51. С. 178–186.
2. *Липенков В.Я., Саламатин А.Н.* Релаксационное расширение ледяного керна из буровой скважины на станции Восток // Антарктика: Доклады комиссии. 1989. Вып. 28. С. 59–72.
3. *Липенков В.Я., Рыскин О.А., Барков Н.И.* О связи между количеством воздушных включений во льду и условиями льдообразования // МГИ. 1999. Вып. 86. С. 75–92.

4. *Alley R.B., Fitzpatrick J.J.* Conditions for bubble elongation in cold ice-sheet ice // Journ. of Glaciology. 1999. V. 45 (149). P. 147–153.
5. *Anderson D.L., Benson C.S.* The densification and diagenesis of snow: properties, processes and applications // Ice and snow: properties, processes, and applications / Ed W.D. Kingery. Cambridge, MA, M.I.T. Press, 1993. P. 391–411.
6. *Arnaud L.* Modelisation de la transformation de la neige en glace a la surface des calottes polaires // These de doctorat, de l'Universite Joseph Fourier de Grenoble, 1997. 297 p.
7. *Arnaud L., Lipenkov V.Ya., Barnola J.M., Gay M., Duval P.* Modeling of the densification of polar firn: characterization of the snow-firn transition // Annals of Glaciology. 1998. V. 27. P. 333–337.
8. *Gow A.J.* Bubbles and bubble pressure in Antarctic glacier ice // CRREL Research Report. 1968. V. 249. 27 p.
9. *Gow A.J., Williamson T.* Gas inclusions in the Antarctic ice sheet and their glaciological significance // Journ. of Geophys. Research. 1975. V. 80 (36). P. 5,101–5,108.
10. *Jouzel J., Barkov N.I., Barnola J.M., Bender M., Chappellaz J., Genton C., Kotlyakov V.M., Lipenkov V., Lorius C., Petit J.R., Raynaud D., Raisbeck G., Ritz C., Sowers T., Stievenard M., Yiou F., Yiou P.* Extending the Vostok ice-core record of palaeoclimate to the penultimate glacial period // Nature. 1993. V. 364 (July 29, 1993). P. 407–412.
11. *Krinner G., Raynaud D., Doutriaux C., Dang H.* Simulations of the Last Glacial Maximum ice sheet surface climate: implications for the interpretation of ice core air content // Journ. of Geophys. Research. 2000. V. 105 (D2). P. 2059–2070.
12. *Lipenkov V.Ya.* Air bubbles and air-hydrate crystals in the Vostok ice core // Physics of ice core records / Ed. T. Hondoh. Sapporo: Hokkaido Univ. Press, 2000. P. 243–282.
13. *Lipenkov V.Ya., Salamatin A.N., Duval P.* Bubbly ice densification in ice sheets: II. Application // Journ. of Glaciology. 1997. V. 43 (145). P. 397–407.
14. *Maeno N., Ebinuma T.* Pressure sintering of ice and its implication to the densification of snow at polar glaciers and ice sheets // Journ. of Phys. Chemistry. 1983. V. 87 (21). P. 4103–4110.
15. *Martinerie P., Raynaud D., Etheridge D.M., Barnola J-M., Mazauder D.* Physical and climatic parameters which influence the air content in polar ice // Earth and Planetary Science Letters. 1992. V. 112. P. 1–13.
16. *Martinerie P., Lipenkov V., Raynaud D., Chappellaz J., Barkov N.I., Lorius C.* Air content paleo record in the Vostok ice core (Antarctica): A mixed record of climatic and glaciological parameters // Journ. of Geophys. Research. 1994. V. 99 (D5). P. 10565–10576.
17. *Ohno H., Lipenkov V.Ya., Hondoh T.* Air bubble to clathrate hydrate transformation in polar ice sheets: A reconsideration based on the new data from Dome Fuji ice core // Geophys. Research Letters. 2004. V. 31. L21401. doi:10.1029/2004GL021151.
18. *Salamatin A.N., Duval P.* Creep flow and pressure relaxation in bubbly medium // Intern. Journ. of Solids and Structures. 1997. V. 34 (1). P. 61–78.
19. *Salamatin A.N., Lipenkov V.Ya., Duval P.* Bubbly ice densification in ice sheets: I. Theory // Journ. of Glaciology. 1997. V. 43 (145). P. 387–396.
20. *Salamatin A.N., Tsyganova E.A., Lipenkov V.Ya., Petit J.R.* Vostok (Antarctica) ice-core time-scale from datings of different origins // Annals of Glaciology. 2004. V. 39. P. 283–292.
21. *Salamatin A.N., Lipenkov V.Ya.* Simple relations for the close-off depth and age in dry-snow densification // Annals of Glaciology. 2008. V. 49. P. 71–76.
22. *Salamatin A.N., Lipenkov V.Ya., Barnola J.M., Hori A., Duval P., Hondoh T.* Snow/firn densification in polar ice // Physics of ice core records / Ed. T. Hondoh. Sapporo: Hokkaido Univ. Press, 2009. V. 2. P. 195–222.
23. *Salamatin A.N., Tsyganova E.A., Popov S.V., Lipenkov V.Ya.* Ice flow line modeling in ice core data interpretation: Vostok Station (East Antarctica) // Physics of ice core records / Ed. T. Hondoh. Sapporo: Hokkaido Univ. Press, 2009. V. 2. P. 167–194.
24. *Saltykov S.A.* Stereometricheskaya metallografiya [Stereometric metallography]. [In Russian]. Moscow: Metallurgiya, 1976. 271 p.
25. *Shieh S.-Y., Evans J.W.* The stability of cylindrical voids and of cylinders subject to temperature gradient // Journ. of Geophys. Research. 1991. V. 72 (16). P. 4093–4100.
26. *Shoji H., Langway C.C.Jr.* Mechanical properties of fresh ice core from Dye 3, Greenland // Greenland Ice Core: Geophysics, Geochemistry, and the Environment / Ed. C.C.Jr. Langway, H. Oeschger, W. Dansgaard. Washington: DC. American Geophysical Union, 1985. P. 39–48. (Geophysical Monograph 33).
27. *Shreve R.L.* Migration of air bubbles, vapor figures, and brine pockets in ice under a temperature gradient // Journ. of Geophys. Research. 1967. V. 72 (16). P. 4093–4100.
28. *Spencer M.K., Alley R.B., Fitzpatrick J.J.* Developing a bubble number-density paleoclimatic indicator for glacier ice // Journ. of Glaciology. 2006. V. 52 (178). P. 358–364.
29. *Stauffer B., Schwander J., Oeschger H.* Enclosure of air during metamorphosis of dry firn to ice // Annals of Glaciology. 1985. V. 6. P. 108–112.
30. *Stehle N.S.* Migration of bubbles in ice under a temperature gradient // Physics of snow and ice: Proc. of international conference on low temperature science (1966). V. 1. Pt. 1 / Ed. H. Ôura. Sapporo: Institute of Low Temperature Science, Hokkaido University, 1967. P. 219–232.
31. *Weertman J.* Bubble coalescence in ice as a tool for the study of its deformation history // CRREL Research Report. 1968. Rep. 251.
32. *Wilkinson D.S., Ashby M.F.* Pressure sintering by power law creep // Acta Metallurgica. 1975. V. 23 (11). P. 1277–1285.

Appendix
Model for compression of a single bubble in the polydisperse bubble-ice system

Formally replacing the ice porosity c by $c\bar{\omega}/\omega$ in the theory of bubbly-ice densification developed for *monosize* bubbles (see Equation (4.6) in [19]), we come to the following integral equation governing the compression of a single bubble in the *polydisperse* bubble-ice system:

$$p_l - p = \frac{2}{\sqrt{3}} \int_{2c\bar{\omega}/\sqrt{3}}^{2\omega/\sqrt{3}} \left[\eta\left(\xi^2 + 4\mathbf{II}_\mathbf{E}\right) + 4\kappa \mathbf{II}_\mathbf{E} \eta'\left(\xi^2 + 4\mathbf{II}_\mathbf{E}\right) \right] d\xi + \tag{A1}$$

$$+ \frac{4}{3}\left(\bar{c\omega} + \frac{3}{2}\varepsilon_1\right) \int_{c\bar{\omega}/\omega}^{1} \left[\eta\left(\frac{4(\bar{c\omega})^2}{3\varsigma^2} + 4\mathbf{II}_\mathbf{E}\right) + \kappa \frac{4(\bar{c\omega})^2}{3\varsigma^2} \eta'\left(\frac{4(\bar{c\omega})^2}{3\varsigma^2} + 4\mathbf{II}_\mathbf{E}\right) \right] d\varsigma;$$

$$\mathbf{II}_\mathbf{E} = \frac{1}{3}\left(\bar{c\omega}\right)^2 + \bar{c\omega}\varepsilon_1 + \varepsilon_a^2.$$

Here $\eta(\xi)$ is the rheological factor (apparent viscosity) in the flow law of pure ice:

$\tau = 2\eta(4\mathbf{II}_\mathbf{E})\dot{\mathbf{e}}$

relating the stress deviator $\mathbf{t}$ to the strain rate tensor $\dot{\mathbf{e}}$. By definition, $\mathbf{II}_\mathbf{E} = 0.5\dot{\mathbf{e}}{:}\dot{\mathbf{e}}$ is the second invariant of

the tensor $\dot{\mathbf{e}}$. Implicitly η additionally depends on the ice temperature T. The tuning parameter κ accounts for different limiting schemes of the ice cell deformation ($0.4 < \kappa < 1$) [18], whilst $\mathbf{II_E}$ is the second invariant of the macro-scale (averaged) strain rates in the two phase bubble-ice system with ε_1 and ε_a being, respectively, the vertical compression rate and the effective strain rate induced by the ice-sheet global flow [19]. The load pressure is given by

$$p_l = p_{atm} + g\rho_i \int_0^h (1-c)\, dh, \qquad \text{(A2)}$$

where p_{atm} is the atmospheric pressure, g is the gravity acceleration, and ρ_i is the density of pure ice.

Expressing the bubble volume v from Equation (7) and using Equation (3), we obtain

$$\omega = \frac{T}{p}\frac{d}{dt}\left(\frac{p}{T}\right). \qquad \text{(A3)}$$

Together with initial conditions at the moment t_d when the bubbly-ice particle is at the end of the disintegration zone ($h = h_d$), Equations (7), (A1) – (A3) form a complete model of the bubble ensemble evolution with time $t > t_d$ as the reference ice layer (particle) sinks into depth h.

In accordance with the general considerations of this paper, the same Equations (7), (A1) – (A3) are valid for the mean ensemble characteristics $\overline{p}$, $\langle v \rangle$, and $\overline{\omega}$ substituted for p, v, and ω, respectively, provided that v_0 in Equation (7) is replaced by $\gamma_0/N\rho_i$, where γ_0 is the dimensionless genetic parameter of bubbly-ice densification dealing with amount of air trapped in an ice particle: $\gamma_0 = V\rho_i$.

By definition,

$c = N\rho_i\langle v \rangle/(1 + N\rho_i\langle v \rangle)$,

and the averaged form of Equation (10) yields

$c = \gamma_c/(\gamma_c + \overline{p})$, $\gamma_c = p_0 T\gamma_0/T_0$.

Correspondingly, we come to an exact replication of the bubbly-ice densification model developed by Salamatin with coauthors [19].

Установившееся распределение пузырьков воздуха по размерам в рекристаллизационном льду

Лёд полярных ледников характеризуется обилием включений (пузырьков) атмосферного воздуха, которые формируются в результате закрытия сообщающихся пор на завершающей стадии рекристаллизационного льдообразования. В слое ледника, залегающем между границей фирн–лёд и началом зоны трансформации газовых включений в гидраты воздуха, геометрические параметры включений (счётная концентрация и средний размер пузырьков) определяются температурой фирна и скоростью аккумуляции льда в период льдообразования, а также сжатием включений в процессе уплотнения ледникового льда после закрытия пор. Последнее означает, что для использования размеров пузырьков в качестве палеоклиматических индикаторов их необходимо предварительно привести к условиям (температуре, давлению атмосферного воздуха) на границе фирн–лёд, что, в свою очередь, требует знания закономерностей изменения распределения пузырьков по размеру на разных глубинах в теле полярного ледника.

В основу теоретического анализа эволюции ансамбля газовых включений положена модель уплотнения пузырькового льда [13, 19], которая в данном приложении использована для описания релаксационного сжатия пузырьков, входящих в различные размерные группы. Теоретическое рассмотрение проблемы привело к заключению об инвариантности формы распределения пузырьков по размеру в стационарных климатических условиях. Этот вывод был подтверждён результатами измерений газовых включений во льду голоценового возраста и в слое льда, сформировавшегося в районе станции Восток в период последнего максимума оледенения (примерно 28–16 тыс. лет назад). Кроме этого, было установлено, что включения воздуха, формирующиеся во льду в разных климатических условиях, также характеризуются практически одинаковым распределением по относительному размеру.

Показано, что распределения нормированных радиусов газовых пузырьков, измеренных на различных глубинах в шести пунктах Антарктиды и Гренландии, близко соответствуют логнормальному закону и характеризуются практически одинаковым стандартным отклонением, равным 0,38±0,05. Инвариантность распределения пузырьков по относительному размеру означает существование связи между приведённым к условиям на границе фирн–лёд средним радиусом включений и их счётной концентрацией, что подтверждается экспериментальными данными.

На основании результатов выполненного исследования разработан простой метод приведения геометрических параметров включений воздуха к известным условиям в момент замыкания фирновых пор, который открывает перспективу одновременного использования двух экспериментально независимых характеристик пузырьков (счётной концентрации и среднего размера) для реконструкции условий льдообразования (температуры и скорости аккумуляции льда).